Applied Geochemistry 147 (2022) 105502

Contents lists available at ScienceDirect

Applied Geochemistry

journal homepage: www.elsevier.com/locate/apgeochem

Day-night alternation and effect of sulfate ions on photodegradation of triclosan in water

Yi Liu [a,b,c,1], Yiqun Wang [a,b,c,d,1], Biao Jin [a,b,c,*], Ziwei Wang [a,b,c], Sasho Gligorovski [a,b,d], Davide Vione [e], Yifeng Zhang [e], Ping'an Peng [a,b,d], Gan Zhang [a,b]

[a] State Key Laboratory of Organic Geochemistry, Guangzhou Institute of Geochemistry, Chinese Academy of Sciences, Guangzhou, 510640, China
[b] CAS Center for Excellence in Deep Earth Science, Guangzhou, 510640, China
[c] University of Chinese Academy of Sciences, Beijing, 10069, China
[d] Guangdong-Hong Kong-Macao Joint Laboratory for Environmental Pollution and Control, Guangzhou Institute of Geochemistry, Chinese Academy of Science, Guangzhou, 510640, China
[e] DTU Environment, Department of Environmental Engineering, Technical University of Denmark, 2800 Kgs. Lyngby, Denmark

ARTICLE INFO

Keywords:
Stable isotope
Water pollution
Degradation
Transformation products

ABSTRACT

Photodegradation is an essential process for the in-stream elimination of triclosan (TCS). There are still some knowledge gaps concerning reaction kinetics, pathways, and transformation products, which are important for understanding the environmental fate of TCS. For example, the effects of ionic strength and day-night alternation on TCS photodegradation have been barely considered in previous studies. To fill these gaps, this study assesses the effect of sulfate ions (SO_4^{2-}) on the photodegradation of TCS under day-night shifts. Compound-specific carbon and chlorine isotope analysis were applied to characterize different bond-cleavage pathways. Moreover, variations in TCS reaction products distribution were analyzed by using Fourier transform ion cyclotron resonance mass spectrometry. A numerical model was developed to describe the concentration and stable carbon isotopic evolution of TCS under different conditions. Based on the observed experimental data, we show that SO_4^{2-} can affect the kinetics and product distribution during the photodegradation of TCS. In particular, sulfate ions (100 mM) inhibited the yield of the toxic product, 2,8-dichlorodibenzo-p-dioxin (2,8-DCDD). Furthermore, day-night alternations lead to different predominant bond-cleavage pathways depending on sulfate concentration. By so doing, we propose a realistic framework for the direct photodegradation of TCS in sunlit natural surface waters.

1. Introduction

Triclosan (TCS) is a high-production volume chemical compound, which is used as antimicrobial agent in numerous consumer products. Due to extensive use and ineffective removal by wastewater treatment processes, TCS is widespread in different aquatic systems including river, lake, groundwater, and sea (Liu et al., 2022; Singer et al., 2003; Zhao et al., 2010, 2013). Wastewater discharge is a major source accounting for TCS ubiquity in the water environment (García et al., 2014). Furthermore, TCS has been prioritized among the persistent, mobile and toxic (PMT) substances, due to its high risk to the drinking water resources (Schulze et al., 2018). According to the European Union - Water Framework Directive, environmental standards for TCS are 0.1 and 0.28 μg L^{-1} (annual mean and 95th percentile, respectively; Northern Ireland, 2015). Moreover, toxic phototransformation products of TCS such as chlorinated phenols and polychlorinated dibenzo-p-dioxins (PCDD) are formed during natural photolytic attenuation (Buth et al., 2009; Lores et al., 2005; Sola-Gutierrez et al., 2020; Wu et al., 2019), and also during remediation processes such as electrochemical oxidation and photocatalysis (Schröder et al., 2020; Schroder et al., 2021; Sola-Gutierrez et al., 2018; Xu et al., 2020). In order to better characterize TCS phototransformation processes associated with toxic by-products, the photolytic transformation of TCS in water has been investigated in the laboratory by applying different light

* Corresponding author. State Key Laboratory of Organic Geochemistry, Guangzhou Institute of Geochemistry, Chinese Academy of Sciences, Guangzhou, 510640, China.
E-mail address: jinbiao@gig.ac.cn (B. Jin).
[1] The first two authors contributed equally to this study.

https://doi.org/10.1016/j.apgeochem.2022.105502
Received 12 May 2022; Received in revised form 26 October 2022; Accepted 27 October 2022
Available online 5 November 2022

sources and varying experimental conditions (Bianco et al., 2015; Gautam et al., 2014; Lam et al., 2020; Sanchez-Prado et al., 2006; Sola-Gutierrez et al., 2020). Information obtained from these studies is essential to advance mechanistic understanding of light-induced transformation pathways of TCS. In particular, the main TCS photodegradation pathways are reaction with hydroxyl radicals ($^{\bullet}$OH), direct photolysis, and reaction with organic matter triplet excited states (^{3}DOM*). The first two processes would prevail in waters with low dissolved organic carbon, the last one in high-DOC waters. Furthermore, differently from $^{\bullet}$OH, direct photolysis and DOM* reaction would produce PCDD (Bianco et al., 2015).

Increasing research interests have recently arisen about the in-stream attenuation of organic micropollutants (Glaser et al., 2020; Muller et al., 2020; Schmitt et al., 2021). Among different natural elimination processes that take place in water, light-induced degradation is important for many trace organic pollutants (Vione and Scozzaro, 2019). In the case of TCS, the photo-induced cleavage of different bonds might lead to preferential production of different toxic intermediates; therefore, previous studies have focused on product identification and characterization (Apell et al., 2020; Wu et al., 2019). Moreover, compounds specific isotope analysis (CSIA) has been increasingly applied as an emerging tool to characterize light-induced transformation pathways of different organic pollutants including chlorobenzenes (Passeport et al., 2018), brominated phenols (Zakon et al., 2013), and polychlorinated biphenyls. In a recent study, carbon CSIA was applied to elucidate the main bond-cleavage pathways for TCS under different pH conditions, and in presence of dissolved organic matter (Liu et al., 2020a). Different extents of carbon isotope fractionation have been reported, which suggests important variations in predominant bond-cleavage pathways.

The in-stream natural attenuation of organic pollutants from wastewater is a reactive transport process (Liu et al., 2020b), which is affected by both photolytic and biogeochemical reactions. Alternation of day-night conditions may be very important, but it was rarely considered in previous studies, and its impact on TCS photolytic transformations is still unclear. Furthermore, sulfate ions (SO_4^{2-}) concentrations in freshwaters have increased globally over the last decades, as a consequence of the rising trend of atmospheric sulfur (S) depositions into fresh waters across large parts of North America, Europe, and Asia (Zak et al., 2021). For instance, in the period from 1950s to 2010s, sulfate concentration in Lake Taihu in China continuously increased until it reached levels of about 100 mg L^{-1}, due to increasing SO_2 emissions caused by coal consumption in this region (Tao et al., 2013). The SO_4^{2-} concentrations typically range between 0 and 630 mg L^{-1} in rivers, from 0 to 250 mg L^{-1} in lakes, and from 0 to 230 mg L^{-1} in groundwater. Moreover, sulfate is typically present at 2.7 g L^{-1} concentration in seawater (Zak et al., 2021). Sulfate ions can affect terrestrial and freshwater ecosystems, but their impact on the environment is still poorly characterized. For example, some previous studies have shown that sulfate ions can affect the multiphase and heterogeneous processes of organic pollutants in cloud water, and in aerosol deliquescent particles (Loisel et al., 2021; Mekic and Gligorovski, 2021; Mekic et al., 2020; Wang et al., 2021a). Here, for the first time to our knowledge, we evaluated the effect of sulfate ions on TCS photochemical degradation, relevant to freshwater and seawater. In fact, the main goal of our study is to evaluate the impacts of day-night alternation and sulfate ions on TCS photodegradation kinetics and pathways. Specifically, we conducted laboratory experiments by altering the light irradiance to simulate natural sunlight shifts. The FT-ICRMS and carbon CSIA techniques were applied as useful tools, to probe comprehensive composition of organic photoproducts, as well as bond-cleavage reaction pathways. We aim to better understand the impact of day-night shifts and sulfate ions on *(i)* the kinetics of TCS photochemical degradation, *(ii)* the prevailing bond-cleavage pathways, and *(iii)* the transformation products distribution.

2. Experimental section

2.1. Chemicals and solvents

Triclosan (TCS, > 99.8%) and hexamethylbenzene (HMB, > 99.8%) standards were purchased from Sigma-Aldrich (Germany). Sodium sulfate was purchased from Aladdin (China). Methanol (>99.8%, Merck, Germany), isooctane (>99.8% Aladdin, China) and ethyl acetate (>99.8%, Aladdin, China) were all of HPLC grade. Ultrapure water (18.2 MΩ cm, Sartorius, Germany) was used to prepare aqueous solutions. Standard stock solution (10 g L^{-1}) of TCS was prepared in methanol, and stored at 4 °C in the dark. This procedure is enabled by the fact that previous studies have shown that the direct photolysis of TCS does not involve $^{\bullet}$OH radicals (Kliegman et al., 2013), which would be scavenged by methanol. The stock solution was diluted 1000 times with water for the irradiation experiments.

2.2. Experimental setup

The experimental setup used to simulate solar transformation of TCS mainly includes a light source and a glass reactor. Specifically, the experimental light source uses a high-pressure xenon lamp (500 W) equipped with a filter (300–700 nm), to generate UV-VIS radiation that is very close to natural sunlight (Liu et al., 2020a). The photoreactor is a double-layered borosilicate glass chamber. The outer chamber of the glass reactor was filled and circulated with water at a constant temperature (292.15 K), and a magnetic stirrer with rotor was used to homogenize the solution.

A 10 mg L^{-1} aqueous solution of TCS was irradiated for 10.5 h, to simulate the daytime period of the winter solstice in Guangzhou in 2020. To simulate the night period, the reactor was wrapped in aluminum foil and placed in the dark at 19 °C for 13.5 h. The irradiation was applied again on the second day for 10.5 h, and then the reactor was kept in the dark for 13.5 h. The total experimental time was 48 h. The pH of the irradiated solutions was fixed at 8, with sodium dihydrogen phosphate as the buffer. In these conditions, the protonated and deprotonated forms of TCS have comparable concentration, but the direct photolysis process largely involves deprotonated TCS (see Fig. S1 in the Supplementary Material, hereinafter SM). Aqueous samples were taken at different time intervals, and were immediately stored at 4 °C for subsequent sample treatment and analysis. In order to evaluate the effect of sulfate ions on the photodegradation of TCS, the sulfate concentrations in this study varied between 1.2 mM and 100 mM.

2.3. Analytical approach

2.3.1. Sample preparation and extraction

The detailed sample extraction procedures have been described in our previous study (Liu et al., 2020a). Briefly, water samples were first added with concentrated sulfuric acid to obtain protonated TCS. Samples were then extracted three times using 3 mL of ethyl acetate. The collected ethyl acetate fractions were evaporated and dissolved with isooctane. Prior to instrumental analysis, hexamethylbenzene (HMB) was added as an internal standard.

2.3.2. TCS concentration determination

The quantitative analysis of TCS in solution was carried out with gas chromatography mass spectrometry (GC-MS, QP2020NX; Shimadzu, Kyoto, Japan), which was operated in selected ion monitoring (SIM) mode. Gas chromatographic separation was conducted using a DB-5MS capillary column (30 m × 0.25 mm × 0.25 mm; Agilent, Santa Clara, USA). A volume of 1 mL treated sample (isooctane) was injected in splitless mode. Helium was used as the carrier gas, with a constant flow rate of 1.2 mL min^{-1}.

2.3.3. Product analysis by FT-ICRMS

Transformation products during photodegradation of TCS have been assessed by Fourier transform ion cyclotron resonance mass spectrometry (FT-ICRMS), which is the state-of-the-art instrument that has sufficient mass resolution to separate and precisely assign elemental compositions for organic compounds. Therefore, it provides qualitative information about molecular composition of samples. A key advantage of FT-ICR MS is that it does not need preliminary separation by liquid chromatography in order to simplify the system, thereby ensuring comprehensive identification of ionizable intermediates (in the case of LC-MS, many of them might be lost because they are not properly eluted by LC).

Aqueous samples were collected at scheduled time intervals during photolytic transformation of TCS, and immediately analyzed by using a solariX XR FT-ICR MS (Bruker Daltonik GmbH, Bremen, Germany), with a refrigerated, 9.4 T actively shielded superconducting magnet (Bruker Biospin, Wissembourg, France), and a Paracell analyzer cell. The samples were ionized by an electrospray ionization (ESI) ion source (Bruker Daltonik GmbH, Bremen, Germany).

The most probable formulas for the detected ions were estimated by software, using a mass tolerance of ±1 ppm. The maximum number of atoms was set as follows: 30 ^{12}C, 60 ^{1}H, 20 ^{16}O, 3 ^{14}N, 1 ^{32}S, 1 ^{13}C, 1 ^{18}O, and 1 ^{34}S. The aromaticity equivalent (*Xc*) equation (**Eq-1**) (Yassine et al., 2014) was applied to improve the identification and characterization of aromatic and polyaromatic compounds that contain C, H, O, and N atoms.

$$Xc = \frac{2C + N - H - 2mO - 2nS}{DBE - mO - nS} + 1 \quad \text{(Eq-1)}$$

where *m* and *n* represent the fractions of, respectively, oxygen and sulfur atoms that are involved in the π-bonds of a molecular structure. The values of *m* and *n* were set to 0.5, because the negative mode of ESI is most sensitive to compounds that contain carboxylic functional groups. Threshold values of *Xc* between 2.5 and 2.7 ($2.5 \leq Xc < 2.7$), and equal to or higher than 2.7 ($Xc \geq 2.7$) were chosen as minimum criteria for the respective presence of aromatics or multicore aromatic (polyaromatic) compounds (e.g., TCS dimers) in the identified ions (Yassine et al., 2014).

2.3.4. Compound specific isotope analysis

Stable carbon isotope analysis was performed using a gas chromatograph, connected to an isotope ratio mass spectrometer via GC-IsoLink (GC-IRMS, Thermo Fisher Scientific, USA), and equipped with a DB-5MS capillary column (30 m × 0.25 mm × 0.25 mm; Agilent, Santa Clara, USA). The samples were pre-concentrated, and then injected in splitless mode. The inlet temperature was 300 °C. The oven temperature of the GC was programmed as mentioned above for concentration determination. The chlorine isotope ratios of TCS were determined using a GC-qMS method, which has been described and validated in our previous study (Liu et al., 2021). The description of this approach and key instrumental parameters is available in SM.

2.4. Modeling approach

2.4.1. Reaction kinetic modeling

A numerical model was developed to simulate TCS concentration variation. The transformation process was mathematically described with first-order kinetics, by considering continuous day-night shifts:

$$\frac{d[TCS]}{dt} = -\sum_{i=1}^{n} r_{day_i} - \sum_{j=1}^{m} r_{night_j} \quad \text{(Eq-2)}$$

$$r_{day_i} = k_{day_i} \cdot [TCS] \quad \text{(Eq-3)}$$

$$r_{night_j} = k_{night_j} \cdot [TCS] \quad \text{(Eq-4)}$$

where r [h^{-1}] is the reaction rate of TCS during the specific day "i" or night "j", and k [h^{-1}] is the corresponding first-order rate constant during the specific day or night.

2.4.2. Stable carbon isotope fractionation modeling

Modeling of carbon isotopic evolution of TCS was conducted by using a first-principle based numerical approach, as described and applied in previous studies (Buchner et al., 2017; Eckert et al., 2012; Jin et al., 2013; Jin and Rolle, 2016). The carbon isotope fractionation factor, α, is defined as the ratio between the first-order rate coefficients of heavy (H) and light (L) TCS isotopologues:

$$\alpha_{day_i} = \frac{{}^{H}k_{day_i}}{{}^{L}k_{day_i}} \quad \text{(Eq-5)}$$

$$\alpha_{night_j} = \frac{{}^{H}k_{night_j}}{{}^{L}k_{night_j}} \quad \text{(Eq-6)}$$

$$k_{day_i} = {}^{L}k_{day_i} \cdot \frac{{}^{L}[TCS]}{[TCS]} + {}^{H}k_{day_i} \cdot \frac{{}^{H}[TCS]}{[TCS]} \quad \text{(Eq-7)}$$

$$k_{night_j} = {}^{L}k_{night_j} \cdot \frac{{}^{L}[TCS]}{[TCS]} + {}^{H}k_{night_j} \cdot \frac{{}^{H}[TCS]}{[TCS]} \quad \text{(Eq-8)}$$

where k represents first-order rate coefficients of light or heavy TCS isotopologues during the ith day or the jth night. The TCS concentration is the sum of the light and heavy TCS isotopologues.

$$R_{TCS} = \frac{{}^{H}[TCS]}{{}^{L}[TCS]} \quad \text{(Eq-9)}$$

$$\delta_{TCS} = \frac{R_{TCS} - R_{STD}}{R_{STD}} \quad \text{(Eq-10)}$$

where R_{TCS} (unitless) stands for TCS isotope ratios at different reaction time; R_{STD} is the isotope ratio of the isotopic standard material; δ represents TCS stable isotope (carbon or chlorine) values in delta notation.

The reaction rate constant "k" and fractionation factor "α" were obtained by searching the best-fit of the experimental data based on a trust-region-reflective method for the minimization of the non-linear least squares.

3. Results and discussion

3.1. Reaction kinetics

Transformation of TCS under light irradiation was observed in aqueous solution in the absence and in the presence of sulfate ions, during the period of two days and two nights. The photolysis rate constant of TCS in sulfate-free solution was 8.4×10^{-6} s^{-1} during the first day of light irradiation (Fig. 1a, Fig. S3). During the second day, a first order rate constant of 1.0×10^{-5} s^{-1} was observed.

Additional experiments were carried out in the presence of 1.2 and 100 mM of SO_4^{2-}. The two selected sulfate concentrations represent, respectively, the monitored average sulfate level in the Pearl River (Southern China) (data not shown), and the level of sulfate that provides ionic strength high enough to affect the phototransformation of some organic compounds (Buchner et al., 2017; Eckert et al., 2012). Indeed, it has been shown that ionic strength may affect the photochemical degradation of organic compounds in fresh waters and marine waters (Parker et al., 2013). In this study, during the first day of light irradiation of TCS in the aqueous phase, a slight increase of the first order rate constants was observed in the presence of 1.2 mM SO_4^{2-} ($k_{1st} = 9.9 \times 10^{-6}$ s^{-1}), and in the presence of 100 mM SO_4^{2-} ($k_{1st} = 1.1 \times 10^{-5}$ s^{-1}) (see Table 1).

In contrast, during the second day, the first order rate constant of TCS

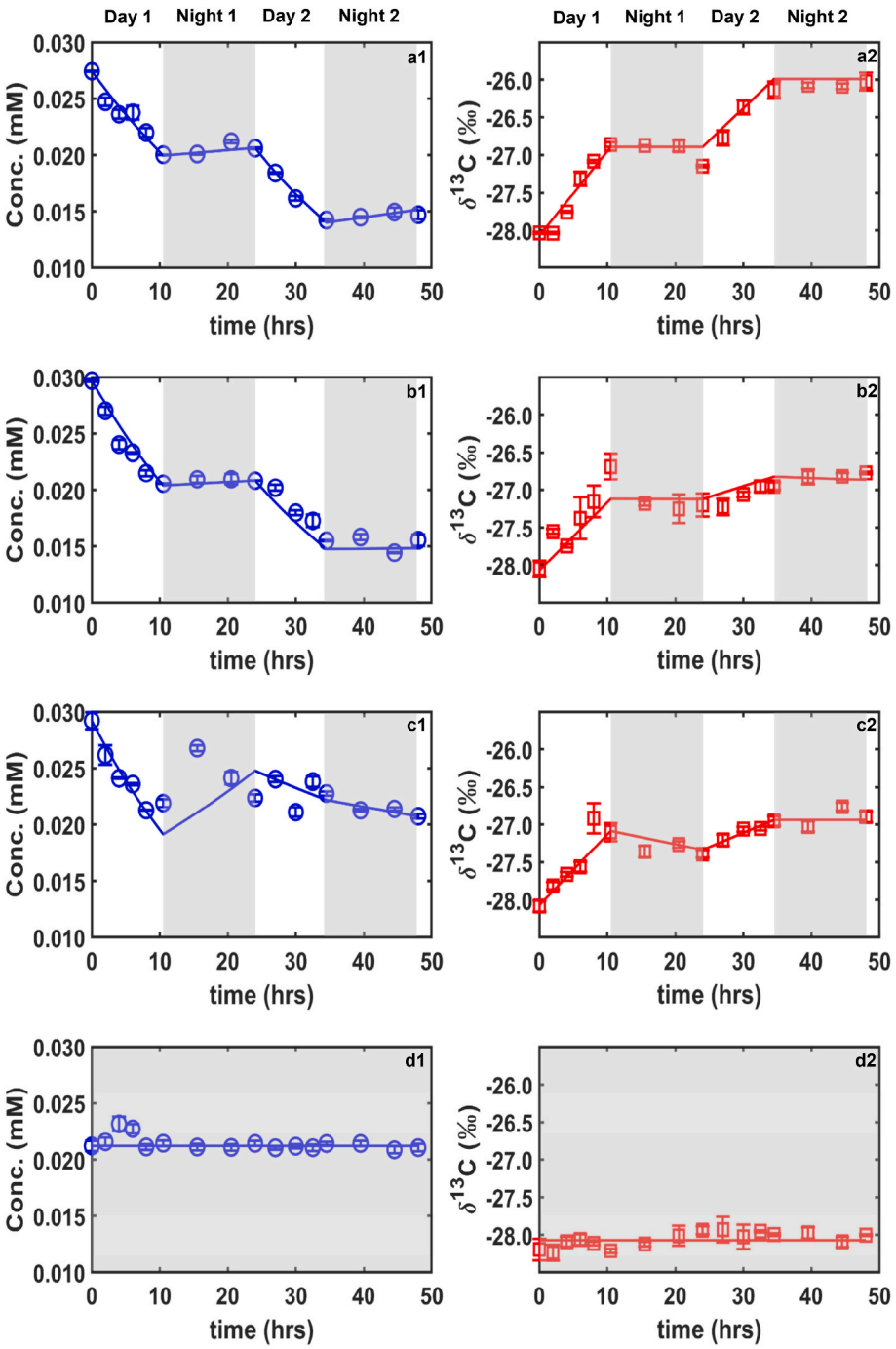

Fig. 1. Photodegradation patterns of TCS obtained during day-night shifts. Panels a1-d1 represent TCS concentration variations (a1) in sulfate-free solution, (b1) in the presence of 1.2 mM SO_4^{2-}, (c1) in the presence of 100 mM SO_4^{2-}, (d1) is the control experiment, i.e., TCS dissolved in water and always kept in the dark at constant temperature (292.15 K). Panels a2-d2 show the carbon isotope fractionation of residual TCS in the corresponding experimental conditions. The symbols represent the observed experimental data, and the solid lines are the simulated results by the model. The shaded zones represent simulated night time.

decreased slightly to 9.2×10^{-6} s^{-1} (1.2 mM SO_4^{2-}), and to 2.9×10^{-6} s^{-1} (100 mM SO_4^{2-}) (Fig. 1c, Fig. S3). Similarly, a decrease of the rate constant of vanillin was observed at higher ionic strength, when adjusted by sulfate ions (Loisel et al., 2021). It has been shown that ionic strength affects a reaction, because each ion is surrounded by an extended solvation shell that can influence the ionic activities and the reaction rates (Herrmann, 2003; Liu et al., 2003). When neutral reactants participate in the reaction as it is the case in this study, the ionic-strength dependence of the reaction rate is determined by the change in the activity coefficients of the neutral reactants (Herrmann, 2003). Under dark conditions during Day 1 and Day 2, negligible TCS degradation was observed. In contrast, at a sulfate concentration of 100 mM (Fig. 1c), the TCS concentration increased slightly on Night 1, indicating a recovery phenomenon. Similarly, a rapid photohydration of a potent endocrine-disrupting compound such as trenbolone acetate (TBA) was followed by a significant regrowth during the night, under conditions representative of surface waters (pH 7, 25 °C) (Qu et al., 2013). In the following sections, the impact of sulfate ions on TCS degradation mechanisms under day-night shifts are evaluated and discussed.

3.2. Bond-cleavage pathway and stable isotope effects

As shown in Fig. 1 (a2-c2), significant carbon isotope fractionation occurred during TCS photo transformation, due to preferential cleavage of ^{12}C-containing reactive bonds. This means that residual TCS was enriched in ^{13}C. Generally, carbon isotope fractionation of TCS on Day 1 was more significant compared with Day 2. During Day 1, the observed

Table 1
The determined carbon isotope fractionation factors (ε_C) and apparent kinetic isotope effects ($AKIE_C$) (the calculation schemes are available in SM), based on the experimental data.

Experiment	SO_4^{2-} (mM)	Time	k × 10^{-6} (s^{-1})	Half-life (days)	ε_C (‰)	$AKIE_C$
1	0	day 1	8.4	0.9	−3.80 ± 0.01	1.048 ± 0.0001
		day 2	10.2	0.8	−2.40 ± 0.04	1.030 ± 0.0005
2	1.2	day 1	9.9	0.8	−2.60 ± 0.02	1.032 ± 0.0002
		day 2	9.2	0.9	−1.10 ± 0.06	1.013 ± 0.0007
3	100	day 1	11.2	0.7	−2.40 ± 0.03	1.030 ± 0.0004
		day 2	2.9	2.8	−3.70 ± 0.10	1.046 ± 0.0012

$\delta^{13}C$ values varied from −28.04‰ to −26.86‰ (no sulfate), −28.05‰ to −26.69‰ (1.2 mM sulfate), and −28.08‰ to −27.10‰ (100 mM sulfate). Moreover, sulfate addition resulted in slightly lower carbon isotope enrichment factor on Day 1, compared with the sulfate-free experiments. In order to further characterize possible bond-cleavage processes of TCS at "Day 1" and "Day 2" with different concentrations of sulfate ions, we evaluated individual values of apparent kinetic isotope effect (AKIE) (see Table 1; the calculation schemes are available in SM). For the sulfate-free experiment, the AKIE value for "Day 1" was about 1.048, which is quite close to the theoretical carbon kinetic isotope effect for C–Cl bond cleavage (i.e. 1.057), derived from Streitwieser Semiclassical theory (Elsner, 2005). Therefore, dechlorination via C–Cl bond cleavage could be the main TCS transformation pathway on Day 1, to produce monochlorinated and/or dichlorinated products in agreement with the FT-ICRMS analysis (see Fig. 3a1). However, the AKIE values decreased to 1.03 on Day 2, which is more consistent with C–H bond cleavage (theoretical value of 1.021) as the main reaction mechanism. A previous study suggested that C–H bond cleavage could be the possible isotope-sensitive step for TCS polymerization (Liu et al., 2020a), forming polycyclic aromatic compounds. Indeed, the CHOCl compounds formed during "Day 2" are depicted in region II, and they correspond to aromatic compounds exhibiting a certain degree of unsaturation (see Fig. 3a2 and related discussion, in section "Products Identification by FT-ICRMS").

The photolytic degradation of TCS upon addition of sulfate ions exhibited similar AKIE values in Day 1 at both concentrations (1.032 at 1.2 mM sulfate, and 1.030 at 100 mM). This finding would be consistent with C–H and, possibly, also C–Cl bond cleavage as primary isotope-sensitive steps. However, in the presence of 100 mM SO_4^{2-}, the AKIE values varied from 1.030 at Day 1–1.046 at Day 2. The latter value could be attributed to ether (i.e. C–O) bond cleavage, which would preferentially produce chlorophenols and chlorobenzenes from TCS (see section "Products Identification by FT-ICRMS"). However, in the presence of 1.2 mM SO_4^{2-}, the AKIE value obtained on Day 2 decreased to 1.013, which is similar to the value of the sulfate-free experiment, and suggests an important role of C–H bond cleavage.

A possibility to highlight different reaction pathways is given by the carbon-chlorine dual isotope plots (Fig. 2). The traces relative to "Day 1" and "Day 2" overlap at least partially (i.e., they have the same slope) if the same overall pathway is operational in both days, while they are distinct (different slopes) if the pathways are different. An examination of Fig. 2 suggests that different pathways between Day 1 and Day 2 were likely to be operational in the cases of no sulfate (Figs. 2a) and 100 mM SO_4^{2-} (Fig. 2c), while the same pathway likely occurred for 1.2 mM SO_4^{2-} (Fig. 2b).

Concerning photolytic dechlorination of TCS, sulfate addition could stimulate carbon-chlorine bond cleavage, as indicated by the smaller

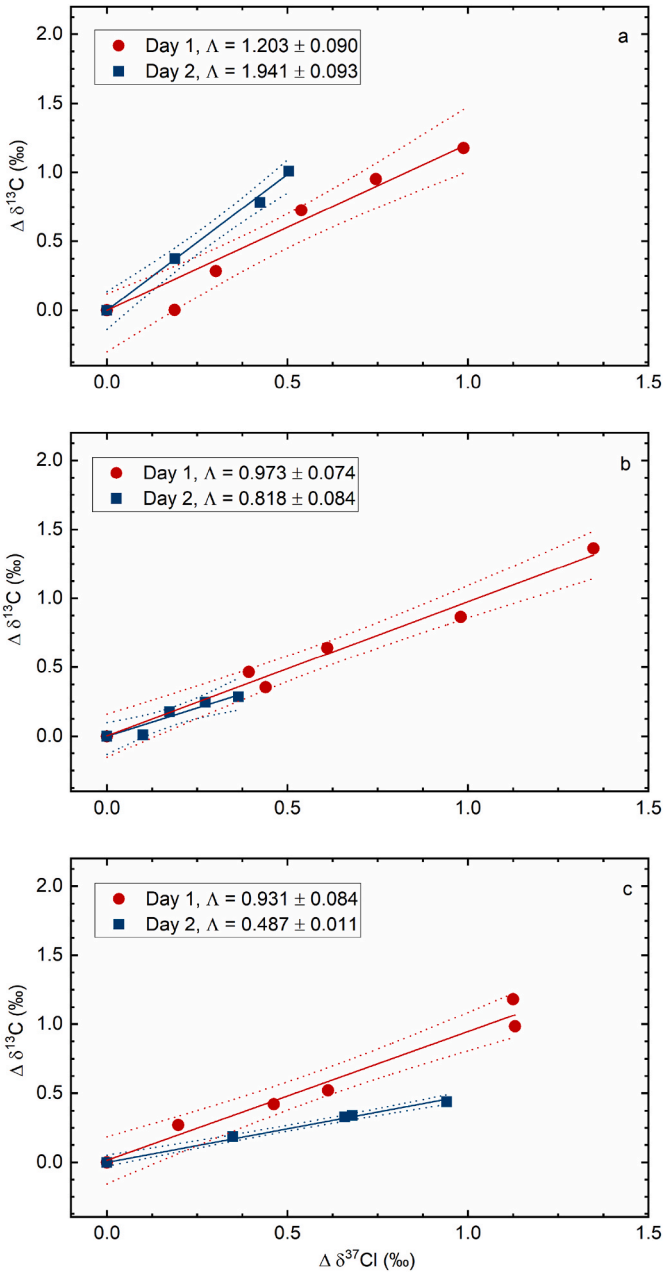

Fig. 2. Carbon-chlorine dual isotope plots obtained during TCS photo-transformation, (a) in sulfate-free solutions, (b) in the presence of 1.2 mM sulfate ions, and (c) in the presence of 100 mM sulfate ions. Λ is the line slope.

dual-isotope slope values compared with the sulfate-free experiment. The strongest TCS dechlorination was observed on "Day 2" of the experiment at 100 mM sulfate, while the sulfate-free experiment resulted in much lower TCS dechlorination on "Day 2". These data suggest that variation in bond-cleavage reaction pathways is an interplay between day-night alternation and the levels of sulfate ions. Given that different bond-cleavage pathways could lead to different transformation products in aqueous solution, the effect of sulfate on TCS photodegradation products during "Day 1" and "Day 2" is discussed in the following section.

3.3. Products Identification by FT-ICRMS

The analysis of the product compounds formed by photodegradation of TCS was performed in the absence of sulfate ions, and in the presence

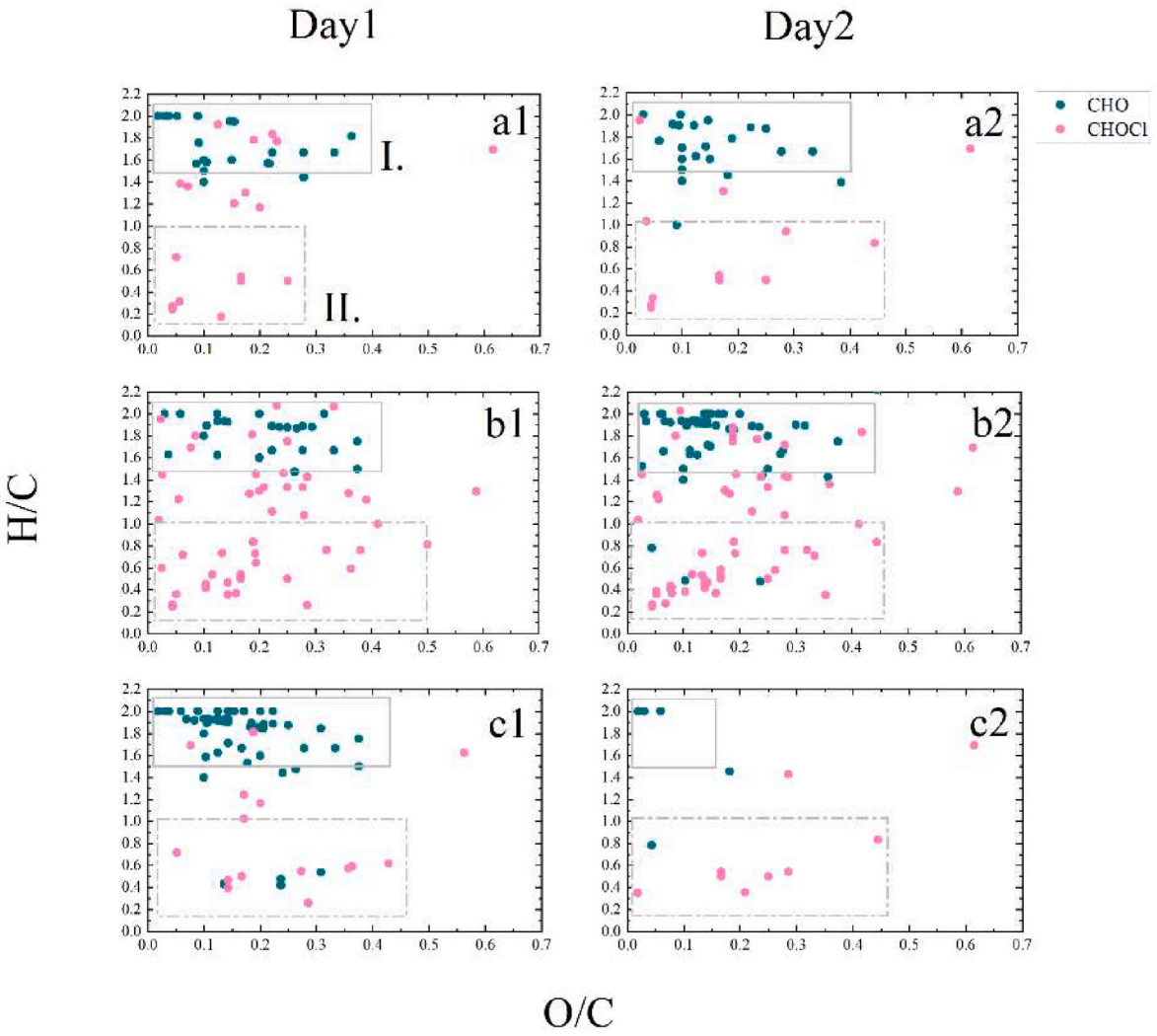

Fig. 3. Van Krevelen plot of the CHO and CHOCl product compounds, formed upon photodegradation of TCS during "Day 1" and "Day 2", (a) in sulfate-free solutions, (b) in the presence of 1.2 mM SO_4^{2-}, and (c) in the presence of 100 mM SO_4^{2-}. The solid rectangle labeled as "I" contains compounds with H/C $\geq$ 1.5 and O/C $\leq$ 0.5, whereas the dash-dotted rectangle identifies region "II", which includes compounds with H/C $\leq$ 1 and O/C $\leq$ 0.5.

of 1.2 and 100 mM of sulfate ions. Fig. 3 shows typical van Krevelen plots in form of H/C *versus* O/C atom number ratios, which provide an average overview of the product characteristics.

Two regions have been labeled as I and II, referring to, respectively, H/C $\geq$ 1.5 and O/C $\leq$ 0.5 (I), as well as H/C $\leq$ 1 and O/C $\leq$ 0.5 (II). Cyclic, saturated, and unsaturated aliphatic compounds are located in region I, while the compounds in region II would be aromatic hydrocarbons with low oxygen content (Wang et al., 2021b).

In sulfate-free TCS aqueous solution during Day 1 (Fig. 3a1), CHO compounds are mainly located in region I, whereas CHOCl compounds occur in both region I and region II. During "Day 2" (Fig. 3a2), the CHO and CHOCl compounds are separated more clearly in regions I and II, respectively. There is no significant change in the number of product compounds, between Day 1 and Day 2. In the presence of 1.2 mM of sulfate ions, the number of detected product compounds increases significantly during both days, compared to the case of sulfate-free aqueous solution (Fig. 3b1, b2). This is particularly true in the case of CHOCl compounds, the number of which is similar in Day 1 and Day 2, and always higher compared to no-sulfate conditions. In contrast, the number of CHO compounds does not change much in Day 1 with 1.2 mM SO_4^{2-}, compared to no sulfate, but a considerable increase is observed in Day 2 (Fig. 3b2).

The results observed with 100 mM sulfate are very different from those with 1.2 mM sulfate. In Day 1, one observes a huge number of CHO compounds (Fig. 3c1), which decrease considerably in Day 2 (Fig. 3c2). The CHOCl compounds are not very different from the case of no sulfate in Day 1, and they are slightly fewer in Day 2.

Intriguingly, elevated sulfate concentration substantially decreases the number of detected product compounds upon prolonged photooxidation. This finding suggests that high loads of sulfate ions may help eliminate many products, formed by photodegradation of TCS. For example, the concentration of the toxic product 2,8-dichlorodibenzo-p-dioxin (2,8-DCDD) decreases substantially, in the presence of 100 mM sulfate ions (see Fig. S5).

The *Xc* parameters (see **Eq-1**) (Kourtchev et al., 2016; Wang et al., 2017; Yassine et al., 2014) were evaluated under different experimental conditions, in order to characterize the molecular structures of the detected products, and provide potential insights into the reaction pathways. Fig. 4 shows the difference in the number of observed CHO compounds, between "Day 1" and "Day 2". In the absence of sulfate ions, there was only slight difference between the CHO product compounds detected in "Day 1" and "Day 2". The addition of sulfate ions drastically changed the characteristics of the observed CHO compounds.

In the presence of 1.2 mM SO_4^{2-}, the number of produced CHO compounds increased significantly during "Day 2", compared to "Day 1" (Fig. 4b1 and b2). The number of aliphatics, aromatics and, most

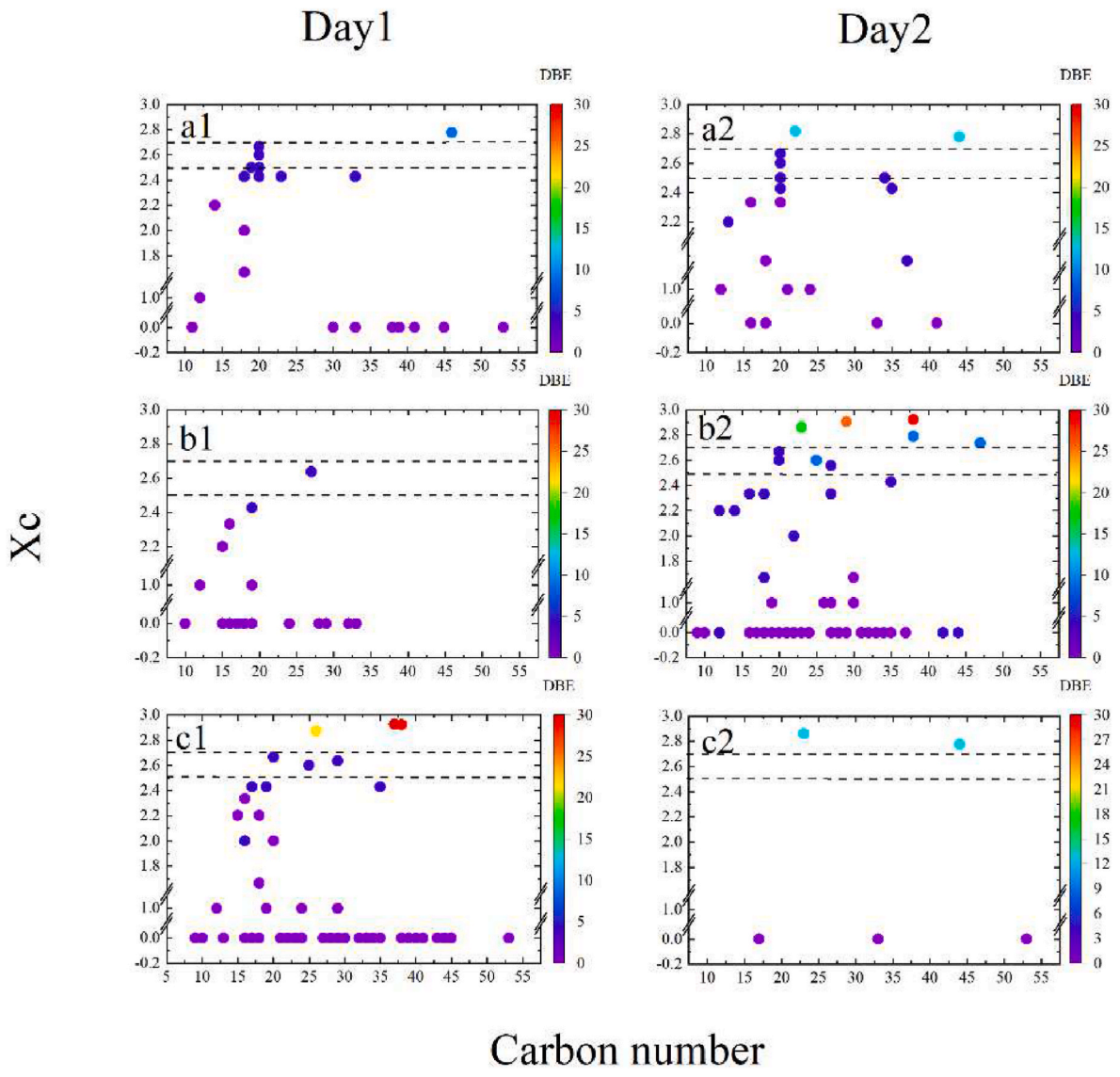

Fig. 4. Carbon number vs. Xc plot for the CHO products, obtained upon photodegradation of TCS in sulfate-free solution (panel a), in the presence of 1.2 mM sulfate (panel b), and in the presence of 100 mM sulfate (panel c). The two columns (a1-c1; a2-c2) represent the CHO products formed during "Day 1" and "Day 2", respectively. The color coding indicates variation of DBE values for individual CHO products.

notably, condensed aromatic compounds (compounds with more than one ring structure, and an oxygenated functional group such as carbonyl) increased, indicating that 1.2 mM SO_4^{2-} can facilitate oligomerization processes (Loisel et al., 2021; Mekic et al., 2020; Wang et al., 2021b). When comparing "Day 2" (Fig. 4b2) with "Day 1" (Fig. 4b1), one sees an increase of the compounds with low DBE values (DBE $\leq$5) and Xc = 0, i.e., saturated long-chain aliphatic compounds.

In the presence of higher sulfate concentration (100 mM), the number of detected CHO compounds significantly decreased during "Day 2", compared to "Day 1". In particular, aliphatic compounds with Xc < 2.5 were absent in "Day 2" (Fig. 4c(1–2)). Moreover, during "Day 1", three compounds with DBE>20 and $X_c > 2.7$ appeared (unsaturated polyaromatic compounds) (Tong et al., 2016), but they were absent in "Day2". The plots depicting the carbon number *vs.* Xc, for the CHOCl products obtained upon photodegradation of TCS in the absence and in the presence of sulfate ions, are shown in SM (Fig. S4). These observations indicate that the concentration of sulfate ions can alter both the kinetics of TCS photodegradation, and the distribution of products. Interestingly, sulfate has been reported to also affect the kinetics of methoxyphenols transformation, and the subsequent product distribution (Loisel et al., 2021; Wang et al., 2021b). Here we show that a combination of irradiation and SO_4^{2-} could affect both the kinetics, and the products distribution of TCS phototransformation. In particular, high sulfate levels could inhibit formation of the toxic product 2,8-DCDD (see Fig. 5), the formation of which became insignificant with 100 mM SO_4^{2-}.

The formation of 2,8-DCDD requires C–H and C–Cl bond breaking (see Scheme S1). In contrast, ether (C–O) bond cleavage would produce monoaromatic compounds, and would not yield 2,8-DCDD. As shown in Section 3.2, elevated sulfate concentration can enhance C–O cleavage at the expense of the other processes, thereby inhibiting the formation of 2,8-DCDD. The effects of sulfate on C–O cleavage can be easily accounted for, if this process is heterolytic (see Scheme S1). In this case, the ionic strength associated to 100 mM SO_4^{2-} would facilitate charge separation. The alternative pathway (homolytic C–O cleavage) would produce a phenoxy radical, which has tendency to dimerize and produce multicore aromatics, which is not supported by FT-ICRMS findings.

Finally, the chlorophenolic compounds detected by FT-ICRMS undergo fast photodegradation at pH 8, involving loss of chlorine (Vione et al., 2007), which could account for the small number of

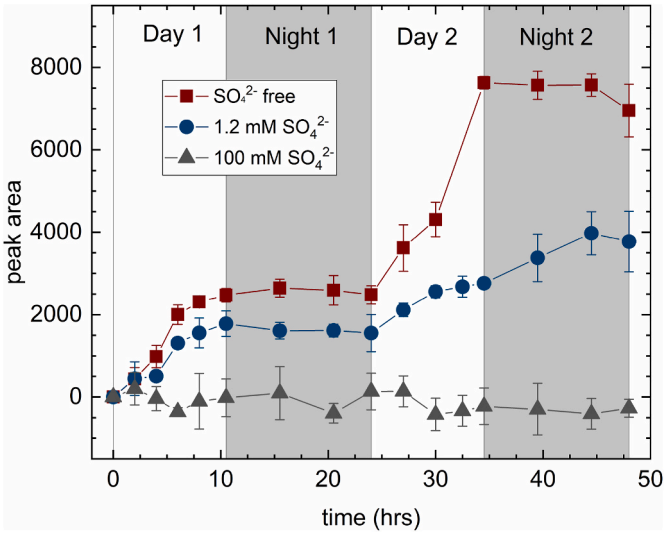

Fig. 5. Formation of 2,8-dichlorodibenzo-p-dioxin (2,8-DCDD), during TCS phototransformation under day-night alternations, in the absence of sulfate, and in the presence of different sulfate concentrations.

transformation intermediates, and the important degree of dechlorination found with 100 mM SO_4^{2-} (Fig. 3c2, 4c). As an alternative, some of the many CHO compounds initially formed at elevated SO_4^{2-} concentration (Fig. 3c1) might act as photosensitizers (e.g., quinones) (Maurino et al., 2011), and induce different TCS phototransformation pathways than those leading to 2,8-DCDD.

4. Conclusion

Increasing use of TCS as antimicrobial agent in various customer products resulted in its ubiquitous presence in natural waters. Photolytic transformation is one of the most important processes for the in-stream natural attenuation of TCS. However, phototransformation products such as 2,8-DCDD are of environmental concern, since they are even more persistent and toxic than TCS. Here we show that irradiation and SO_4^{2-} could affect the kinetics and the products distribution of TCS phototransformation.

Based on the data obtained from carbon and chlorine CSIA, as well as products FT-ICRMS analysis, we found that 100 mM SO_4^{2-} favored ether (C–O) bond cleavage of TCS, therefore breaking TCS down into monoaromatic compounds. Such a process would inhibit the formation of 2,8-DCDD that, on the contrary, requires C–H and C–Cl bond breaking (see Scheme S1). If the C–O breaking process is heterolytic, it can be enhanced by the ionic strength associated to 100 mM SO_4^{2-}, which facilitates charge separations. To wrap up, we proposed a realistic framework for light-induced natural attenuation of TCS in surface waters, and therefore improving mechanistic understanding on the corresponding bond-cleavage reaction pathways. Future studies are importance to characterize possible impacts induced by different ions in water on TCS phototransformation.

Notes

The authors declare no competing financial interest.

Declaration of competing interest

The authors declare that they have no known competing financial interests or personal relationships that could have appeared to influence the work reported in this paper.

Data availability

Data will be made available on request.

Acknowledgements

The study is funded by the scientific instrument developing project of the Chinese Academy of Sciences (Grant NO. 282021000003). B.J. acknowledges support from National Key Research and Development Plan (2019YFC1805500), Guangdong Foundation for Science and Technology Research (2020B1212060053; 2019A1515011035), and grant from State Key Laboratory of Organic Geochemistry, Chinese Academy of Sciences (SKLOG2020-4). S.G. acknowledges following projects: the Chinese Academy of Science, INTERNATIONAL COOPERATION Grant (132744KYSB20190007), National Natural Science Foundation of China (41773131, 41977187), and National Key Research and Development Program (2017YFC0210103). The authors thank Dr. Bin Jiang, Dr. Shutao Gao and Dr. Qiang Wang for assisting with FT-ICRMS and stable isotope analysis.

Appendix A. Supplementary data

Supplementary data to this article can be found online at https://doi.org/10.1016/j.apgeochem.2022.105502.

References

Apell, J.N., Kliegman, S., Sola-Gutierrez, C., McNeill, K., 2020. Linking triclosan's structural features to its environmental fate and photoproducts. Environ. Sci. Technol. 54, 14432–14441.
Bianco, A., Fabbri, D., Minella, M., Brigante, M., Mailhot, G., Maurino, V., Minero, C., Vione, D., 2015. New insights into the environmental photochemistry of 5-chloro-2-(2,4-dichlorophenoxy)phenol (triclosan): reconsidering the importance of indirect photoreactions. Water Res. 72, 271–280.
Buchner, D., Jin, B., Ebert, K., Rolle, M., Elsner, M., Haderlein, S.B., 2017. Experimental determination of isotope enrichment factors – bias from mass removal by repetitive sampling. Environ. Sci. Technol. 51, 1527–1536.
Buth, J.M., Grandbois, M., Vikesland, P.J., McNeill, K., Arnold, W.A., 2009. Aquatic photochemistry of chlorinated triclosan derivatives: potential source of polychlorodibenzo-p-dioxins. Environ. Toxicol. Chem. 28, 2555–2563.
Eckert, D., Rolle, M., Cirpka, O.A., 2012. Numerical simulation of isotope fractionation in steady-state bioreactive transport controlled by transverse mixing. J. Contam. Hydrol. 140–141, 95–106.
Elsner, M., 2005. A new concept linking observable stable isotope fractionation to transformation pathways of organic pollutants. Environ. Sci. Technol. 39, 6896–6916.
García, S., Pinto, G., García-Encina, P., Irusta, R., 2014. Ecotoxicity and environmental risk assessment of pharmaceuticals and personal care products in aquatic environments and wastewater treatment plants. Ecotoxicology 23, 1517–1533.
Gautam, P., Carsella, J.S., Kinney, C.A., 2014. Presence and transport of the antimicrobials triclocarban and triclosan in a wastewater-dominated stream and freshwater environment. Water Res. 48, 247–256.
Glaser, C., Zarfl, C., Werneburg, M., Böckmann, M., Zwiener, C., Schwientek, M., 2020. Temporal and spatial variable in-stream attenuation of selected pharmaceuticals. Sci. Total Environ. 741, 139514.
Herrmann, H., 2003. Kinetics of aqueous phase reactions relevant for atmospheric chemistry. Chem. Rev. 103, 4691–4716.
Northern Ireland, 2015. The water framework directive (classification, priority substances and shellfish waters) regulations (northern Ireland). Statutory Rules of Northern Ireland. Environ. Protect. 351, 58, 2015.
Jin, B., Rolle, M., 2016. Position-specific isotope modeling of organic micropollutants transformation through different reaction pathways. Environ. Pollut. 210, 94–103.
Jin, B., Haderlein, S.B., Rolle, M., 2013. Integrated carbon and chlorine isotope modeling: applications to chlorinated aliphatic hydrocarbons dechlorination. Environ. Sci. Technol. 47, 1443–1451.
Kliegman, S., Eustis, S.N., Arnold, W.A., McNeill, K., 2013. Experimental and theoretical insights into the involvement of radicals in triclosan phototransformation. Environ. Sci. Technol. 47, 6756–6763.
Kourtchev, I., Godoi, R.H.M., Connors, S., Levine, J.G., Archibald, A.T., Godoi, A.F.L., Paralovo, S.L., Barbosa, C.G.G., Souza, R.A.F., Manzi, A.O., Seco, R., Sjostedt, S., Park, J.H., Guenther, A., Kim, S., Smith, J., Martin, S.T., Kalberer, M., 2016. Molecular composition of organic aerosols in central Amazonia: an ultra-high-resolution mass spectrometry study. Atmos. Chem. Phys. 16, 11899–11913.
Lam, K.Y., Nélieu, S., Benoit, P., Passeport, E., 2020. Optimizing constructed wetlands for safe removal of triclosan: a box–behnken approach. Environ. Sci. Technol. 54, 225–234.

Liu, Y., Sheaffer, R.L., Barker, J.R., 2003. Effects of temperature and ionic strength on the rate and equilibrium constants for the reaction I•aq + I-aq ↔ I2•-aq. J. Phys. Chem. 107, 10296–10302.
Liu, Y., Mekic, M., Carena, L., Vione, D., Gligorovski, S., Zhang, G., Jin, B., 2020a. Tracking photodegradation products and bond-cleavage reaction pathways of triclosan using ultra-high resolution mass spectrometry and stable carbon isotope analysis. Environ. Pollut. 264, 114673.
Liu, Y., Zarfl, C., Basu, N.B., Cirpka, O.A., 2020b. Modeling the fate of pharmaceuticals in a fourth-order river under competing assumptions of transient storage. Water Resour. Res. 56, 1–19.
Liu, Y., Liu, S., Wang, Q., Gligorovski, S., Zhang, G., Jin, B., 2021. Stable chlorine isotope analysis of triclosan using GC-qMS: method development and applications. Appl. Geochem. 129, 104961.
Liu, X., Tu, M., Wang, S., Wang, Y., Wang, J., Hou, Y., Zheng, X., Yan, Z., 2022. Research on freshwater water quality criteria, sediment quality criteria and ecological risk assessment of triclosan in China. Sci. Total Environ. 816, 151616.
Loisel, G., Mekic, M., Liu, S., Song, W., Jiang, B., Wang, Y., Deng, H., Gligorovski, S., 2021. Ionic strength effect on the formation of organonitrate compounds through photochemical degradation of vanillin in liquid water of aerosols. Atmos. Environ. 246, 118140.
Lores, M., Llompart, M., Sanchez-Prado, L., Garcia-Jares, C., Cela, R., 2005. Confirmation of the formation of dichlorodibenzo-p-dioxin in the photodegradation of triclosan by photo-SPME. Anal. Bioanal. Chem. 381, 1294–1298.
Maurino, V., Bedini, A., Borghesi, D., Vione, D., Minero, C., 2011. Phenol transformation photosensitised by quinoid compounds. Phys. Chem. Chem. Phys. 13, 11213–11221.
Mekic, M., Gligorovski, S., 2021. Ionic strength effects on heterogeneous and multiphase chemistry: clouds versus aerosol particles. Atmos. Environ. 244, 117911.
Mekic, M., Zeng, J., Zhou, W., Loisel, G., Jin, B., Li, X., Vione, D., Gligorovski, S., 2020. Ionic strength effect on photochemistry of fluorene and dimethylsulfoxide at the air–sea interface: alternative formation pathway of organic sulfur compounds in a marine atmosphere. ACS Earth. Space. Chem. 4, 1029–1038.
Muller, M.E., Werneburg, M., Glaser, C., Schwientek, M., Zarfl, C., Escher, B.I., Zwiener, C., 2020. Influence of emission sources and tributaries on the spatial and temporal patterns of micropollutant mixtures and associated effects in a small river. Environ. Toxicol. Chem. 39, 1382–1391.
Parker, K.M., Pignatello, J.J., Mitch, W.A., 2013. Influence of ionic strength on triplet-state natural organic matter loss by energy transfer and electron transfer pathways. Environ. Sci. Technol. 47, 10987–10994.
Passeport, E., Zhang, N., Wu, L., Herrmann, H., Sherwood Lollar, B., Richnow, H.H., 2018. Aqueous photodegradation of substituted chlorobenzenes: kinetics, carbon isotope fractionation, and reaction mechanisms. Water Res. 135, 95–103.
Qu, S., Kolodziej, E.P., Long, S.A., Gloer, J.B., Patterson, E.V., Baltrusaitis, J., Jones, G.D., Benchetler, P.V., Cole, E.A., Kimbrough, K.C., Tarnoff, M.D., Cwiertny, D.M., 2013. Product-to-Parent reversion of trenbolone: unrecognized risks for endocrine disruption. Science 342, 347–351.
Sanchez-Prado, L., Llompart, M., Lores, M., Garcia-Jares, C., Bayona, J.M., Cela, R., 2006. Monitoring the photochemical degradation of triclosan in wastewater by UV light and sunlight using solid-phase microextraction. Chemosphere 65, 1338–1347.
Schmitt, M., Wack, K., Glaser, C., Wei, R., Zwiener, C., 2021. Separation of photochemical and non-photochemical diurnal in-stream attenuation of micropollutants. Environ. Sci. Technol. 55, 8908–8917.
Schröder, S., San-Román, M.-F., Ortiz, I., 2020. Photocatalytic transformation of triclosan. React. Products. Kinetics. 10, 1468. Catalysts.
Schroder, S., San-Roman, M.F., Ortiz, I., 2021. Dioxins and furans toxicity during the photocatalytic remediation of emerging pollutants. Triclosan as case study. Sci. Total Environ. 770, 144853.
Schulze, S., Sättler, D., Neumann, M., Arp, H.P.H., Reemtsma, T., Berger, U., 2018. Using REACH registration data to rank the environmental emission potential of persistent and mobile organic chemicals. Sci. Total Environ. 625, 1122–1128.
Singer, H., Müller, S., Tixier, C., Pillonel, L., 2003. Triclosan: occurrence and fate of a widely used biocide in the aquatic environment: field measurements in wastewater treatment plants. Surf. Waters. Lake Sediments. 36, 4998–5004.
Sola-Gutierrez, C., San Roman, M.F., Ortiz, I., 2018. Fate and hazard of the electrochemical oxidation of triclosan. Evaluation of polychlorodibenzopdioxins and polychlorodibenzofurans (PCDD/Fs) formation. Sci. Total Environ. 626, 126–133.
Sola-Gutierrez, C., Schroder, S., San-Roman, M.F., Ortiz, I., 2020. Critical review on the mechanistic photolytic and photocatalytic degradation of triclosan. J. Environ. Manag. 260, 110101.
Tao, Y., Yuan, Z., Fengchang, W., Wei, M., 2013. Six-decade change in water chemistry of large freshwater Lake Taihu, China. Environ. Sci. Technol. 47, 9093–9101.
Tong, H., Kourtchev, I., Pant, P., Keyte, I.J., O'Connor, I.P., Wenger, J.C., Pope, F.D., Harrison, R.M., Kalberer, M., 2016. Molecular composition of organic aerosols at urban background and road tunnel sites using ultra-high resolution mass spectrometry. Faraday Discuss 189, 51–68.
Vione, D., Scozzaro, A., 2019. Photochemistry of surface fresh waters in the framework of climate change. Environ. Sci. Technol. 53, 7945–7963.
Vione, D., Minero, C., Housari, F., Chiron, S., 2007. Photoinduced transformation processes of 2,4-dichlorophenol and 2,6-dichlorophenol on nitrate irradiation. Chemosphere 69, 1548–1554.
Wang, X., Hayeck, N., Brüggemann, M., Yao, L., Chen, H., Zhang, C., Emmelin, C., Chen, J., George, C., Wang, L., 2017. Chemical characteristics of organic aerosols in shanghai: a study by ultrahigh-performance liquid chromatography coupled with orbitrap mass spectrometry. J. Geophys. Res. Atmos. 122 (11), 703–711, 722.
Wang, Y., Mekic, M., Li, P., Deng, H., Liu, S., Jiang, B., Jin, B., Vione, D., Gligorovski, S., 2021a. Correction to "ionic strength effect triggers Brown carbon formation through heterogeneous ozone processing of ortho-vanillin. Environ. Sci. Technol. 55, 10186–10187.
Wang, Y., Mekic, M., Li, P., Deng, H., Liu, S., Jiang, B., Jin, B., Vione, D., Gligorovski, S., 2021b. Ionic strength effect triggers Brown carbon formation through heterogeneous ozone processing of ortho-vanillin. Environ. Sci. Technol. 55, 4553–4564.
Wu, J.L., Ji, F., Zhang, H., Hu, C., Wong, M.H., Hu, D., Cai, Z., 2019. Formation of dioxins from triclosan with active chlorine: a potential risk assessment. J. Hazard Mater. 367, 128–136.
Xu, W., Jin, B., Zhou, S., Su, Y., Zhang, Y., 2020. Triclosan removal in microbial fuel cell: the contribution of adsorption and bioelectricity generation. Energies 13, 761.
Yassine, M.M., Harir, M., Dabek-Zlotorzynska, E., Schmitt-Kopplin, P., 2014. Structural characterization of organic aerosol using Fourier transform ion cyclotron resonance mass spectrometry: aromaticity equivalent approach. Rapid Commun. Mass Spectrom. 28, 2445–2454.
Zak, D., Hupfer, M., Cabezas, A., Jurasinski, G., Audet, J., Kleeberg, A., McInnes, R., Kristiansen, S.M., Petersen, R.J., Liu, H., Goldhammer, T., 2021. Sulphate in freshwater ecosystems: a review of sources, biogeochemical cycles, ecotoxicological effects and bioremediation. Earth Sci. Rev. 212, 103446.
Zakon, Y., Halicz, L., Gelman, F., 2013. Bromine and carbon isotope effects during photolysis of brominated phenols. Environ. Sci. Technol. 47, 14147–14153.
Zhao, J.L., Ying, G.G., Liu, Y.S., Chen, F., Yang, J.F., Wang, L., 2010. Occurrence and risks of triclosan and triclocarban in the Pearl River system, South China: from source to the receiving environment. J. Hazard Mater. 179, 215–222.
Zhao, J.L., Zhang, Q.Q., Chen, F., Wang, L., Ying, G.G., Liu, Y.S., Yang, B., Zhou, L.J., Liu, S., Su, H.C., Zhang, R.Q., 2013. Evaluation of triclosan and triclocarban at river basin scale using monitoring and modeling tools: implications for controlling of urban domestic sewage discharge. Water Res. 47, 395–405.